Submitted to the Astrophysical Journal
Preprint typeset using LaTeX style emulateapj v. 5/2/11

HYDROGEN BURNING ON ACCRETING WHITE DWARFS: STABILITY, RECURRENT NOVAE, AND THE POST-NOVAE SUPERSOFT PHASE

William M. Wolf[1], Lars Bildsten[1,2], Jared Brooks[1], and Bill Paxton[2]

Submitted to the Astrophysical Journal

ABSTRACT

We examine the properties of white dwarfs (WDs) accreting hydrogen-rich matter in and near the stable burning regime of accretion rates as modeled by time-dependent calculations done with Modules for Experiments in Stellar Astrophysics (`MESA`). We report the stability boundary for WDs of masses between 0.51 $M_\odot$ and 1.34 $M_\odot$ as found via time-dependent calculations. We also examine recurrent novae that are accreting at rates close to, but below, the stable burning limit and report their recurrence times. Our dense grid in accretion rates finds the expected minimum possible recurrence times as a function of the WD mass. This enables inferences to be made about the minimum WD mass possible to reach a specific recurrence time. We compare our computational models of post-outburst novae to the stably burning WDs and explicitly calculate the duration and effective temperature ($T_{\rm eff}$) of the post-novae WD in the supersoft phase. We agree with the measured turnoff time - $T_{\rm eff}$ relation in M31 by Henze and collaborators, infer WD masses in the 1.0-1.3 $M_\odot$ range, and predict ejection masses consistent with those observed. We close by commenting on the importance of the hot helium layer generated by stable or unstable hydrogen burning for the short- and long-term evolution of accreting white dwarfs.

Subject headings: stars: binaries: close – stars: binaries: symbiotic – stars: novae – stars: cataclysmic variables – stars: white dwarfs – X-rays: binaries

1. INTRODUCTION

The outcome of accretion of hydrogen-rich material onto the surface of a white dwarf (WD) is relevant to classical novae (Gallagher & Starrfield 1978), recurrent novae, supersoft sources (SSS) (van den Heuvel et al. 1992; Nomoto et al. 2007), and even the single degenerate scenario (SDS) for type Ia supernovae progenitors (Nomoto 1982; Nomoto et al. 1984; Cassisi et al. 1998). The outcome depends on the mass of the accreting WD, $M_{\rm WD}$, the accretion rate, $\dot{M}$, and the core temperature, T_c (Sienkiewicz 1980; Townsley & Bildsten 2004; Yaron et al. 2005; Nomoto et al. 2007; Shen & Bildsten 2007). If the accretion rate is too large, the burning can't match it, causing the rapidly accreting matter to pile up into a red giant-like structure (Paczynski & Zytkow 1978; Nomoto et al. 1979). At lower accretion rates, hydrogen can be stably burned to helium at the same rate that is being accreted (Paczynski & Zytkow 1978; Sienkiewicz 1980; Iben 1982; Fujimoto 1982; Paczynski 1983; Livio et al. 1989; Cassisi et al. 1998; Shen & Bildsten 2007; Nomoto et al. 2007). If the accretion rate is lower yet, the hydrogen supply rate is too low to match the stably burning luminosity, so a low-luminosity accreting state is realized while hydrogen accumulates until a thermonuclear runaway occurs, quickly burning the hydrogen and driving a radius increase and mass loss from the WD that appears as a classical or recurrent nova.

Understanding these phenomena first requires understanding the physics of stable burning. Previous studies (Sienkiewicz 1980; Nomoto et al. 2007; Shen & Bildsten 2007) assumed a steady burning state and studied the stability of their solutions in response to linear perturbations. While numerous time-dependent simulations of WDs accreting hydrogen-rich material are already in the literature, many either started with the matter pre-accreted and studied the ensuing outburst or selected initial conditions which are not erased until several flashes have established asymptotic behavior (Iben 1982). Only Paczynski & Zytkow (1978), Sion et al. (1979), Iben (1982), Livio et al. (1989), Shara et al. (1993), Kovetz & Prialnik (1994), Cassisi et al. (1998), and Yaron et al. (2005) examined the time-dependent problem for durations long enough to observe multiple flashes or stable burning. To date, there is no comprehensive time-dependent study of WDs accreting solar composition material over the full range of the stable burning regime for a large range of WD masses. Yaron et al. (2005) was the most complete prior effort, but did not calculate a dense grid in $\dot{M}$ space near the lower stability boundary.

WDs accreting just below the stability boundary will go through periodic hydrogen shell flashes on relatively short timescales, or recurrent novae (RNe). There are currently ten known RNe in our galaxy (Schaefer 2010) with recurrence times on the order of decades. Those RNe with shortest recurrence times have been understood to be massive WDs (see Figure 9 of Nomoto 1982). Since the measured time between outbursts is often an important factor in estimating $M_{\rm WD}$, we require a solid understanding of the mass-recurrence time relation near the lower stability boundary.

At lower $\dot{M}$'s ($\lesssim 10^{-8}\ M_\odot\,{\rm yr}^{-1}$), WDs undergo classical nova cycles whose recurrence times are too long to measure on human timescales (Yaron et al. 2005). Mass determinations of such systems must then rely on other observed parameters. After a CN outburst, the ejected mass is optically thick, obscuring the view of the hot WD

[1] Department of Physics, University of California, Santa Barbara, CA 93106
[2] Kavli Institute for Theoretical Physics, Santa Barbara, CA 93106

below. After a turn-on time, $t_{\rm on}$, the ejecta becomes optically thin, revealing an SSS. Still later, at some turn-off time $t_{\rm off}$ after the outburst, the X-ray luminosity powered by burning in the hydrogen-rich remnant (Starrfield et al. 1974) decreases and the nova event is over. Hachisu & Kato (2010) have offered a way to fit the observed timescales to models in order to infer $M_{\rm WD}$. Tuchman & Truran (1998) and Sala & Hernanz (2005) argue that the mass left in the hydrogen-rich WD envelope after mass loss is determined primarily by $M_{\rm WD}$ and secondarily by the composition of the envelope. This remnant envelope mass is expected to undergo stable hydrogen burning in the post-outburst SSS phase at nearly constant luminosity. If this remaining envelope mass and luminosity are known as a function $M_{\rm WD}$, the duration of the SSS phase can be predicted, allowing a correlation between the measured turn-off time of a CN and $M_{\rm WD}$. With the increasingly large samples of CNe like that of Henze et al. (2011) in M31 and Schwarz et al. (2011) in our own galaxy, we can now test these methods on a meaningful number of CNe.

In this paper, we present models of WDs with masses ranging from $M_{\rm WD} = 0.51\ M_\odot$ to $1.34\ M_\odot$ accreting solar composition material as simulated by `MESA` (Paxton et al. 2011; Denissenkov et al. 2013; Paxton et al. 2013). The conditions for stable hydrogen burning are found, as are the characteristics of unstable models. We compare recurrence times to the previous results from Iben (1982), Livio et al. (1989), Cassisi et al. (1998), and Yaron et al. (2005). We start in §2 by discussing the input physics used to produce the accreting models. Then in §3, we present the relevant background on stable burning as well as the characteristics of our steadily (and stably) burning models. We investigate unstable burning on WDs accreting at rates near, but below, the stable boundary in §4 with comparisons to previous time-dependent calculations explored in §5. We study applications to classical novae in §6, and further implications and questions are addressed in §7, where we comment on the inevitable flashes in the accumulating helium layer.

2. SIMULATION DETAILS AND MODEL BUILDING

Initial WD models were created in `MESA` by evolving stars between 4 and 12 $M_\odot$ from ZAMS through the main sequence, RGB, and AGB through to the white dwarf cooling track. Typically when this is done, very small time steps are required to get through the thermal pulses during the AGB phase. To get around this, the convection in the outer envelope is artificially made more efficient so that the full computations need not be followed (Paxton et al. 2013). Additionally, the larger initial models used enhanced winds to speed up the process, which is why they didn't undergo core collapse. These processes do not impact our results since the physics of interest is in the accreted envelope and nearly independent of the degenerate interior. This process was also used and discussed in Denissenkov et al. (2013).

After the initial WD models were created, they were cooled to a central temperature of $T_c = 3 \times 10^7$ K, hot enough so that the initial flash is not too violent. The results of Yaron et al. (2005) show that for accretion rates in the stable regime, the accumulated Helium layer is at $T \approx 10^8$ K, making the results of hydrogen-rich accretion nearly independent of $T_c < 10^8$ K, a result we also justify in §3. We assume that all WDs are not rotating and that convective overshoot does not occur. To model the nuclear burning, we used `MESA`'s `cno_extras_o18_to_mg26_plus_fe56` network, which accounts for hot CNO burning as well as other heavier isotopes' presence. Radiative opacities are from the OPAL tables (Iglesias & Rogers 1993, 1996). The spatial and temporal resolutions were adjusted to finer and finer levels until no more substantive changes were observed in the stability/instability boundary or in the reported observables (recurrence times, burning layer temperatures, envelope masses, etc.). This typically resulted in models with between 7000 and 10000 mass zones that are dynamically sized in space and time so that a burning region in an active nova or steady burner is well-resolved, typically occupying around half of the mass zones.

The accreted material has solar composition, with $X = 0.70$, $Y = 0.28$, and metal fractions taken from Lodders (2003), though the OPAL opacities assume a different set of metal fractions for solar composition. Initializing the accretion often required irradiating the atmosphere before starting accretion so as to ease the thermal readjustment of the outer layers. Any unphysical effects this would have on the model are undone after the ensuing flash(es) that erase the initial conditions (Paczynski & Zytkow 1978; Sion et al. 1979; Cassisi et al. 1998). The first flash heats the outer layers so that the irradiation is no longer needed for computational convenience. After several flashes (in unstable models) or hydrogen sweeping times, $\Delta M_{\rm H}/(X\dot{M})$, where $\Delta M_{\rm H}$ is the total hydrogen mass (for stably burning models), any hydrogen present in the envelope during the initial accumulation phase has already been burned to helium or ejected. It is after this initial "memory erasing", with irradiation deactivated that we begin our exploration.

For this study, we employ two mass loss prescriptions: super Eddington winds and Roche lobe overflow. For the purposes of our calculation, the RNe systems are assumed to be wide binaries. This is not the case for all RNe. With this assumption, the only active mass loss prescription is the super Eddington wind scheme described in Denissenkov et al. (2013). In this prescription, winds are only active if the photosphereic luminosity of the star exceeds an effective Eddington luminosity which is a mass-average of the local Eddington luminosity from the outer-most cell down to where the optical depth first exceeds 100. The excess luminosity over this effective Eddington luminosity comes in the form of mass ejection moving at the surface escape velocity. Both of these mass ejection scenarios take place over an extended period of time until $L < L_{\rm Edd}$ or $R < R_{\rm RL}$, usually indicating the end of the nova's excursion to the red in the HR diagram. The tighter binaries in which CNe are found can result in either of these ejection scenarios, so we present results with both assumptions in §6, where we also describe the Roche lobe wind prescription in more detail. The inlists for these simulations are available on `http://www.mesastar.org`.

We explore a wide range of WD masses for accretion rates in and near the stable burning regime, so we prepared C-O WDs of masses $0.51\ M_\odot$, $0.60\ M_\odot$, $0.70\ M_\odot$, $0.80\ M_\odot$, $1.00\ M_\odot$, and O-Ne WDs of masses $1.10\ M_\odot$, $1.20\ M_\odot$, $1.30\ M_\odot$, and $1.34\ M_\odot$. Then, using earlier

studies of stability regimes (Sienkiewicz 1980; Nomoto et al. 2007; Shen & Bildsten 2007), we chose accretion rates within and near the stable burning regime. For each WD we then relaxed the accretion rate to the desired rate and allowed the model to evolve for at least 30 envelope turnover times to erase all history, typically accreting $< 10^{-3}\ M_\odot$. While the study of much longer-term accretion is certainly warranted (Cassisi et al. 1998; Piersanti et al. 1999), we wanted to initially avoid introducing significant temporal changes to the models resulting from their increasing mass due to secular accumulation of helium. At the end of this accretion period, we take the measurements shown in Figures 1 and 2.

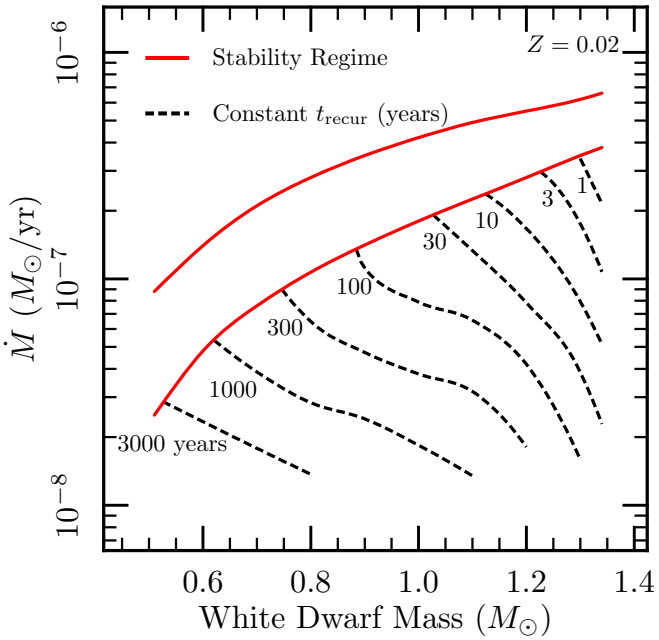

Figure 1. Location of the stable-burning regime on the $M - \dot{M}$ plane. The lower red line represents $\dot{M}_{\rm stable}$, the lowest possible accretion rate which exhibits stable and steady burning for a given WD mass. The upper red line gives the highest such accretion rate, $\dot{M}_{\rm RG}$. WDs accreting at rates above $\dot{M}_{\rm RG}$ will still burn stably, but not at the rate that the matter is being accreted, causing the matter to pile up, forming a red giant-like structure. Also shown in dashed black lines are lines of constant recurrence time (in years) for recurrent novae as interpolated from our grid.

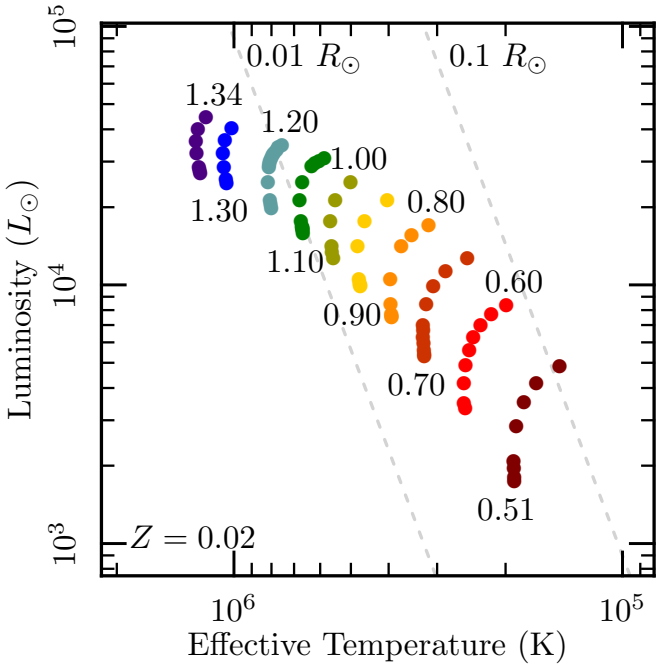

Figure 2. Positions of stable burning models of accreting WDs on the HR diagram. The different colors indicate the different WD masses used in the simulations. Lines of constant radii are drawn for $R = 0.01\ R_\odot$ and $0.1\ R_\odot$. The most luminous point for each mass corresponds to the WD accreting at $\dot{M} = \dot{M}_{\rm stable} + 0.8(\dot{M}_{\rm RG} - \dot{M}_{\rm stable})$. At accretion rates close to $\dot{M}_{\rm RG}$, the radius becomes ill-defined as the envelope slowly expands, so we only report those WDs with well-established radii.

3. STEADILY BURNING MODELS

The conditions for stable burning of hydrogen-rich material are detailed in Shen & Bildsten (2007) for a simple one-zone model of burning. The qualitative results are that steady-state burning becomes stable when an increase in temperature causes the cooling rate to increase more than the energy generation rate. At accretion rates below a certain critical value, $\dot{M}_{\rm stable}$, a temperature perturbation would cause the nuclear heating rate to grow faster than the cooling rate causing a thermonuclear runaway that burns the fuel at a rate faster than accretion, triggering a limit-cycle of accumulation and explosion (i.e. novae). Time-dependent calculations naturally reveal the lower stability bound, as unstable periods of hydrogen burning manifest themselves. Table 1 summarizes these results, indicating the lower limiting accretion rate for stable burning, $\dot{M}_{\rm stable}$, the total mass of hydrogen, $\Delta M_{\rm H}$, the hydrogen sweeping time, $t_{\rm sweep} = \Delta M_{\rm H}/(X\dot{M}_{\rm stable})$, and the luminosity. Additionally, we show the pressure, density, temperature, fraction of pressure due to gas pressure, and hydrogen mass fraction at the point where the exiting luminosity is half of the total luminosity. Finally, we show the thickness of the shell from the half-luminosity point to the surface of the WD as a fraction of the total radius, R, demonstrating that these burning shells are only marginally thin, enhancing their stability. For the range of masses shown in Figure 1, the lower red line represents the values of $\dot{M}_{\rm stable}$. WDs in the region below the lower red line in Figure 1 would be recurrent novae.

The upper edge of the stable regime is more subtle. Fujimoto (1982) and Iben (1982) note that for any WD, there is a maximum envelope mass that can sustain steady-state burning. This corresponds with a plateau in luminosity that is related to the core mass-luminosity relation first found by Paczynski (1970) in AGB cores. In transitioning to a more AGB-like envelope, the luminosity is limited to a maximum value governed by the core mass, and so increasing $\dot{M}$ just causes more matter to pile on to the envelope while steady-state burning at the plateau luminosity continues at the base of the envelope. From this plateau luminosity, we then identify a hydrostatic upper limit to the accretion rate, $\dot{M}_{\rm RG} = L_{\rm plateau}/XQ_{\rm CNO}$. Shen & Bildsten (2007) explicitly showed that this leads to an upper bound on the stable regime that is tightly constrained to $\dot{M}_{\rm RG} \approx 3\dot{M}_{\rm stable}$. It is always the case that $\dot{M}_{\rm RG}$ is a stronger upper limit on the accretion rate than that set by the Eddington luminosity, $\dot{M}_{\rm Edd} = L_{\rm Edd}/XQ_{\rm CNO}$, but in our code it often manifested itself by triggering su-

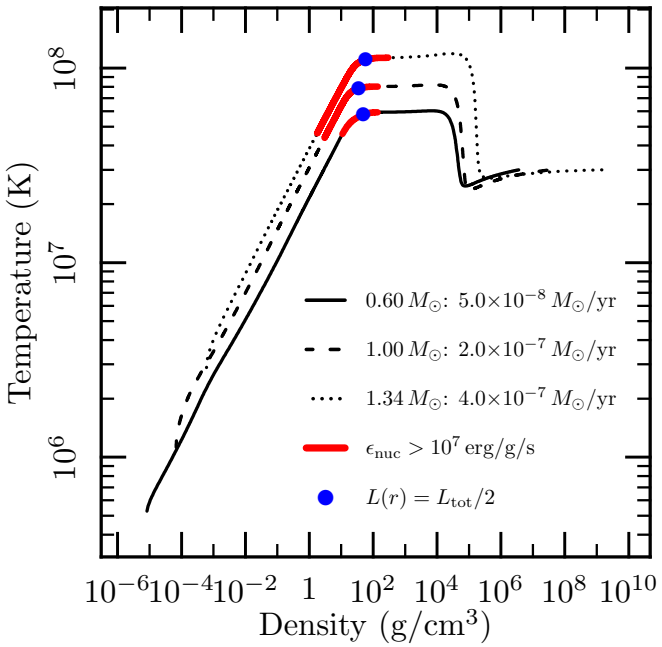

Figure 3. The temperature-density profile of 0.60 $M_\odot$, 1.00 $M_\odot$, and 1.34 $M_\odot$ WDs accreting at $\dot{M} = 5.0 \times 10^{-8}$ $M_\odot$ yr^{-1}, $\dot{M} = 2.0 \times 10^{-7}$ $M_\odot$ yr^{-1}, and $\dot{M} = 4.0 \times 10^{-7}$ $M_\odot$ yr^{-1}, respectively. Areas of significant hydrogen burning are marked, as well as the point where the exiting luminosity is half of the total luminosity of the star.

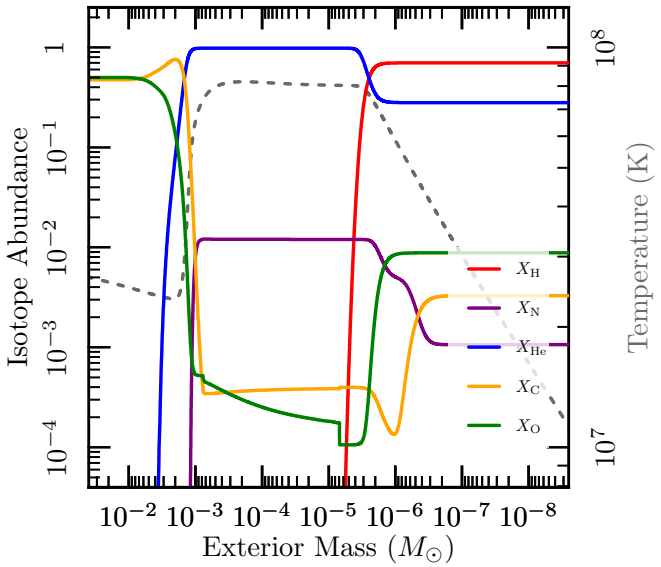

Figure 4. The abundance profile of a 1.00 $M_\odot$ WD accreting at $\dot{M} = 2.0 \times 10^{-7}$ $M_\odot$ yr^{-1}. The temperature profile (dashed line) has also been included to show that the hottest region is the layer of helium ash that dominates the burning conditions rather than the cooler core.

per Eddington winds since the increase in radius caused the opacity in the outer layers to diverge from pure electron scattering.

For a given mass, increasing $\dot{M}$ to $\dot{M}_{\rm RG}$ causes the WD to travel along a path in the HR diagram to higher L and $T_{\rm eff}$ until it hits a "knee", at which point the luminosity continues to grow, but the effective temperature decreases, indicating a radial expansion of the envelope. This knee can be seen in Figure 2. The regime inhabited by these stably and steadily burning WDs in the HR diagram is also known to hold many of the supersoft sources (Nomoto et al. 2007), making these stable burners excellent candidates as the source of the soft X-rays. At high enough $\dot{M}$'s, hydrogen burning cannot burn at the same rate as accretion, causing a radial expansion in the envelope and a build-up of hydrogen (Nomoto et al. 1979). The upper line in Figure 1 represents models with the highest $\dot{M}$ that exhibit steady-state burning of hydrogen at the accreted rate, $\dot{M}_{\rm RG}$. WDs in the region above the upper line in Figure 1 will still burn hydrogen at a constant rate (albeit more slowly than it is being accreted), and their envelopes will grow until optically-thick winds or Roche-lobe overflow can slow the accretion rate (Hachisu et al. 1996). We don't investigate these systems in our study except to find the value of $\dot{M}_{\rm RG}$ for each mass.

The internal structures of 0.60 $M_\odot$, 1.00 $M_\odot$, and 1.34 $M_\odot$ WDs accreting at $\dot{M} = 5.0 \times 10^{-8}$ $M_\odot$ yr^{-1}, 2.0×10^{-7} $M_\odot$ yr^{-1}, and 4.0×10^{-7} $M_\odot$ yr^{-1}, respectively, are shown in Figure 3.

The cores are largely isothermal and degenerate, but on top of them is a hot helium layer that is the ash of the stable burning. Above the ash is the radiative hydrogen envelope with most of the burning occurring just above the Helium ash. To further illustrate the presence of a thick, hot helium layer, Figure 4 shows the elemental abundance and temperature profile of the same 1.00 $M_\odot$ WD shown in Figure 3. Additionally, we see the expected pattern of a hydrogen-helium transition zone above the hot ash, coinciding with a rising ^{14}N mass fraction due to CNO burning.

From Figures 3 and 4 as well as Table 1, we see that there is a temperature $T_{\rm stable}$ at which the stable burning occurs, and that $T_{\rm stable}$ is an increasing function of both $\dot{M}$ and $M_{\rm WD}$. We can explain this dependence with a few assumptions about the nature of the hydrogen-rich envelope. We expect the burning to occur at a depth where the burning timescale, $t_{\rm burn} \sim Q_{\rm CNO}/\epsilon_{\rm CNO}$ (where $\epsilon_{\rm CNO}$ is the nuclear energy generation rate per unit mass and $Q_{\rm CNO}$ is the amount of energy released per unit mass of hydrogen undergoing complete CNO burning) is approximately equal to the accretion timescale, $t_{\rm acc} = \Delta M/\dot{M}$. If we assume a thin shell, where the pressure is approximately $P = GM_{\rm WD}\Delta M/(4\pi R_{\rm core}^4)$, (where $R_{\rm core}$ is the radius at the base of the hydrogen-rich envelope) we get the burning condition to be $\epsilon_{\rm CNO} = (Q_{\rm CNO} G M M_{\rm WD})/(P R_{\rm core}^4)$. Furthermore, the opacity in the hydrogen-rich layer is dominated by electron scattering and the envelope is radiative, so the accretion rate can be related to temperature and pressure via $X Q_{\rm CNO} \dot{M} = L \propto M_{\rm WD} T^4/P$. For our uses, we want to eliminate pressure, so we use $P \propto M_{\rm WD} T^4/\dot{M}$. Finally, we expand $\epsilon_{\rm CNO}$ as a power law in temperature, and with the assumption pressure is due primarily to gas pressure, we may use $\epsilon_{\rm CNO} \propto \rho T^\nu = (P/T) T^\nu = M_{\rm WD} T^{\nu+3}/\dot{M}$. Putting this all together we find

$$T_{\rm stable} \propto \dot{M}^{3/(\nu+7)} M_{\rm WD}^{-1/(\nu+7)} R_{\rm core}^{-4/(\nu+7)}, \qquad (1)$$

where $\nu = 23.58/T_7^{1/3} - 2/3$ and $T_7 = T/10^7$ K as shown in Hansen et al. (2004). Note that $R_{\rm core}$ is negatively correlated with $M_{\rm WD}$ but positively (though weakly) correlated with $\dot{M}$. As a result, we expect $T_{\rm stable}$ to *increase*

Table 1
Properties of Stably Burning WDs at the Stability Boundary

	Stability Boundary				At Half Total Luminosity					
$M_{\rm WD}$ ($M_\odot$)	$\dot{M}_{\rm stable}$ ($10^{-7}\,M_\odot\,{\rm yr}^{-1}$)	$\Delta M_{\rm H}$ ($M_\odot$)	$t_{\rm sweep}$ (yr)	L ($10^3\,L_\odot$)	P (10^{17} dyne/cm^2)	ρ (g/cm^3)	T (10^7 K)	β -	$X_{\rm H}$ -	$\Delta R/R$ -
0.51	0.25	4.9×10^{-5}	2810	1.74	2.31	47.5	5.08	0.928	0.258	0.558
0.60	0.48	2.4×10^{-5}	720	3.36	2.25	36.0	5.69	0.882	0.335	0.496
0.70	0.76	1.2×10^{-5}	226	5.32	2.48	36.7	6.24	0.846	0.286	0.430
0.80	1.07	6.7×10^{-6}	88.7	7.51	2.74	35.9	6.72	0.812	0.290	0.376
0.90	1.41	3.5×10^{-6}	35.4	9.89	3.15	37.0	7.22	0.783	0.291	0.323
1.00	1.80	2.0×10^{-6}	15.5	12.7	3.63	38.9	7.72	0.753	0.280	0.285
1.10	2.40	9.6×10^{-7}	6.08	15.9	4.37	42.1	8.32	0.723	0.272	0.244
1.20	2.80	4.4×10^{-7}	2.24	19.8	5.41	44.8	9.05	0.687	0.284	0.210
1.30	3.50	1.3×10^{-7}	0.534	24.9	7.66	52.4	10.2	0.644	0.293	0.168
1.34	3.80	6.0×10^{-8}	0.226	27.0	9.76	61.0	10.9	0.630	0.290	0.141

with increasing $M_{\rm WD}$ at constant $\dot{M}$ through the implicit $R_{\rm core}$-dependence. For a fixed mass, the radius is approximately constant with changing $\dot{M}$, so $T_{\rm stable}$ is only depending on a small power of $\dot{M}$. Using a prefactor of 3.5×10^8 K (assuming $M_{\rm WD}$ and $R_{\rm core}$ are measured in solar units and $\dot{M}$ in $M_\odot\,{\rm yr}^{-1}$), Equation (1) and the $\nu - T_7$ relation yield temperatures at the point of peak burning accurately to within 20%. For intermediate masses ($0.6\,M_\odot \le M_{\rm WD} \le 1.2\,M_\odot$), the calculated temperatures are typically well within 10% of the simulated values.

4. UNSTABLE BURNING

At accretion rates below the stable burning boundary ($\dot{M} < \dot{M}_{\rm stable}$) indicated in Table 1, the WDs undergo periodic hydrogen flashes. For accretion rates near the stable boundary, these flashes lead to little mass loss from the system. Higher mass WDs experience shorter recurrence times for a given $\dot{M}$. Equivalently, the ignition mass (the mass of accreted material at which a runaway occurs) is smaller for larger core masses where the higher surface gravity allows for higher pressures with less mass accumulation. If we look at the "first unstable model" (the model with $\dot{M} \lesssim \dot{M}_{\rm stable}$), we can identify the minimum recurrence time (or equivalent ignition mass) for that core mass. Before exploring these boundary cases, we should justify our assumption that such a limiting configuration exists

Paczynski (1983) examined flashes on hydrogen-accreting compact objects with a simple one-zone model using linear stability analysis. His analysis showed that as the accretion rate is decreased, the steady state models go from stable (perturbations die exponentially) through quasi-stable (perturbations act as damped oscillators), quasi-unstable (perturbations oscillate with increasing amplitude), and finally fully unstable phases. When simulating the unstable-to-stable flash transition, though, he found that the transformation was very rapid. The one-zone models gave large amplitude flashes (i.e. novae) until the accretion rate reached the stable accretion rate at which point the model switched over to stable and steady burning with very little weakening of the flashes. In other words, there is essentially a discontinuity in the stability of the burning very near $\dot{M}_{\rm stable}$.

In Figure 5 we plot a high resolution grid of $\dot{M}$'s performed on the 1.00 $M_\odot$ model, demonstrating that as $\dot{M}$ approaches $\dot{M}_{\rm stable}$, the igntion mass and recurrence times indeed approach nearly constant values of $\Delta M_{\rm H} \approx 4.4\times10^{-6}\ M_\odot$ and $t_{\rm recur} \approx 40$ days. While we didn't compute this fine of a grid for each mass tested, we obtained the stable/unstable boundary resolved to within five percent of $\dot{M}_{\rm stable}$. This is precise enough for identifying limiting recurrence times and hydrogen ignition masses.

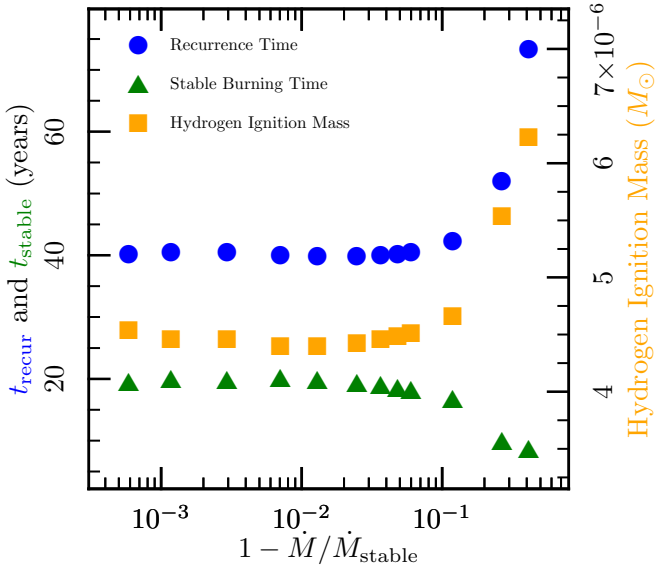

Figure 5. Convergence of the recurrence time, hydrogen ignition mass, and stable burning duration as $\dot{M}$ approaches $\dot{M}_{\rm stable}$ for $M_{\rm WD} = 1.00\ M_\odot$.

An observer can then use an observed nova recurrence time to infer a minimum core mass. Table 2 lists the recurrence times for each first unstable model. There we also list the peak temperature in the helium layer in the low-luminosity state as well as the peak temperature in the burning layer as the convective burning zone develops. The temperature in the helium layer during the low-luminosity state is always close to the extrapolated stable burning temperature (the temperature that would be expected by the empirical power law fit at that $\dot{M}$), though the two temperatures do not track monotonically due to the varying helium mass from model to model.

Townsley & Bildsten (2004) examined how classical novae (CNe) ignition masses depend on $\dot{M}$. Their analysis assumed that the core had reached an equilibrium temperature due to prolonged thermal contact with the cycling outer layers. We see that for sufficiently high $\dot{M}$'s,

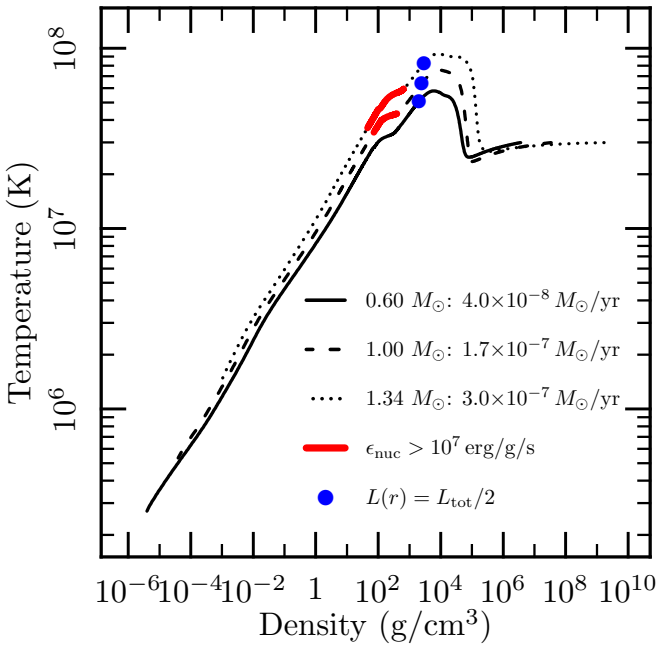

Figure 6. The temperature-density profile of 0.60 $M_\odot$, 1.00 $M_\odot$, and 1.34 $M_\odot$ WDs accreting at $\dot{M} = 3.0 \times 10^{-8}$ $M_\odot$ yr^{-1}, $\dot{M} = 1.7 \times 10^{-7}$ $M_\odot$ yr^{-1}, and $\dot{M} = 3.0 \times 10^{-7}$ yr^{-1}, respectively. Areas of significant CNO burning are marked, as well as the point where the exiting luminosity is half of the total luminosity of the star. These profiles correspond to the quiescent (pre-nova) state of a recurrent nova cycle. The hot helium layer is still present.

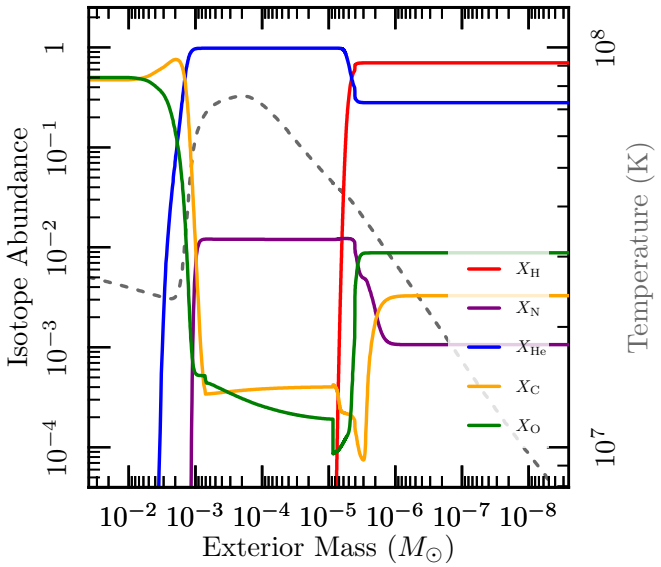

Figure 7. The abundance profile of a 1.00 $M_\odot$ WD accreting at $\dot{M} = 1.7 \times 10^{-7}$ $M_\odot$ yr^{-1}. The temperature profile has also been included to show that the hottest region is the layer of helium ash that dominates the burning conditions rather than the cooler core. Again, this profile is from the quiescent (pre-nova) state.

the helium layer retains a significant fraction of the thermal energy generated in a nova event. So, for these $\dot{M}$'s, the ignition mass and thus nearly all other characteristics of a nova are independent of T_c. This trend is also seen in the models with highest $\dot{M}$'s in Yaron et al. (2005). The hot helium layer in the unstable models is evident in Figures 6 and 7 even while in the quiescent state. For CNe, CNO enrichment is seen in ejecta, indicating that any helium layer from previous outbursts is mixed with the hydrogen during the TNR and ejected along with a portion of the WD core. Thus, we only expect the helium layer to be relevant at $\dot{M}$'s near $\dot{M}_{\rm stable}$ where mixing may cause helium dredge-up, but not necessarily the removal of the entire layer. This would allow for the gradual build-up of an insulating helium layer.

As $\dot{M}$ decreases, more time is allowed for the helium layer to cool. This, in turn, causes the ignition mass to increase, since a higher pressure is required to start a thermonuclear runaway at a lower temperature. The trends for ignition masses in high-mass WDs are shown in Figure 8. Compared to their steadily burning counterparts, the first unstable model (the left-most point for each mass in Figure 8) has a hydrogen ignition mass that is two to three times larger than the stable hydrogen mass. Thus, the static hydrogen masses from the steadily burning masses cannot be extrapolated into the RNe regime to obtain recurrence times.

5. COMPARISONS TO OTHER STUDIES

Sienkiewicz (1980), Shen & Bildsten (2007), and Nomoto et al. (2007) all used linear stability analysis to test the stability of constructed steady-state burning models. This is a time-independent method that serves as a complementary check to our time-dependent calculations. We find that our stability region shown in Figure 1 is largely consistent with these results and plot our results along with those of Nomoto et al. (2007) and Shen & Bildsten (2007). Each of these is plotted in Figure 9, demonstrating the agreement between various techniques.

Shen & Bildsten (2007) studied a one-zone model for stability at various accretion rates and compared their results favorably to those of Nomoto et al. (2007), noting that the discrepancy at lower masses was likely due to their assumption of the burning layer being the mass within a scale height. Nomoto et al. (2007) compute the entire stellar model, but assumed a discontinuous transition from solar composition to nearly pure helium (Nomoto 2012, private communication). We, however, observe a transition zone where most of the burning is occurring, so accurate comparisons are not possible. Nonetheless, Figure 9 demonstrates agreement in the stability boundary between the linear stability analysis and time-dependent calculations.

Table 2
Properties of Recurrent Novae Just Below the Stability Boundary

$M_{\rm WD}$ ($M_\odot$)	$\dot{M}$ ($10^{-7} M_\odot$ yr^{-1})	$t_{\rm recur}$ (yr)	$t_{\rm sweep}$ [a] (yr)	$T_{\rm He}$ [b] (10^7 K)	$T_{\rm peak}$ [c] (10^7 K)
0.51	0.24	4200	2810	5.0	8.3
0.60	0.46	1300	720	5.8	8.8
0.70	0.70	480	226	6.4	9.3
0.80	1.00	200	88.7	7.2	10.0
0.90	1.25	90	35.4	7.0	10.7
1.00	1.7	40	15.6	8.0	11.1
1.10	2.34	13.4	6.08	8.0	12.0
1.20	2.7	4.3	2.24	9.9	13.1
1.30	3.4	1.00	0.534	9.1	14.3
1.34	3.7	0.39	0.226	10.0	15.1

[a] Time for the stable model of the same $M_{\rm WD}$ to burn through one full layer of hydrogen.
[b] Peak temperature during the low-luminosity state in the helium layer.
[c] Peak temperature during the outburst event.

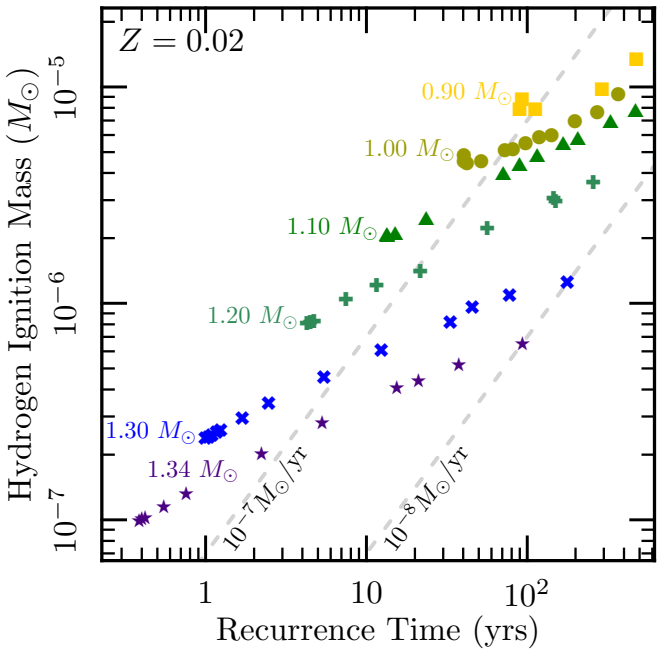

Figure 8. Ignition masses for high-mass WDs as a function of recurrence time. Lines of constant accretion rate (dashed) are also shown. The ignition masses reported here are the total amount of hydrogen accreted between outbursts, $X\dot{M}t_{\rm recur}$, and thus necessarily lower than the total hydrogen mass present at the time of the nova eruption. We find that over the range of $M_{\rm WD}$ and $\dot{M}$ presented here, $\Delta M_{\rm H,tot}/\Delta M_{\rm H,acc} \approx 1.2$.

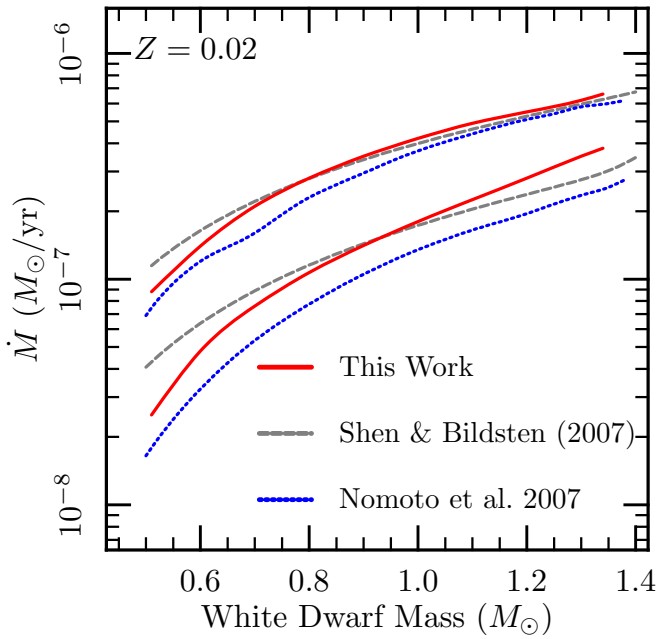

Figure 9. Stability regimes of this work (red solid line), Nomoto et al. (2007) (dotted blue line), and Shen & Bildsten (2007) (dashed gray line).

Other recent time-dependent studies of accreting WDs in and near the stable-burning regime have been carried out by Iben (1982), Livio et al. (1989), Cassisi et al. (1998), and Yaron et al. (2005). The thorough analysis in Iben (1982) shows that recurrence times change over the course of several flashes. Hence, we only compare to simulations that computed through multiple flashes to mitigate the effect of initial condition choices. We now compare our simulations wherever possible.

Iben (1982) studied a 1 $M_\odot$ WD accreting in a quasi-static (hydrostatic) approximation for $\dot{M}$'s near and in the stable-burning regime. He assumed $X = 0.64$ in the accreted material and also neglected mass loss. Both of these assumptions should lead to longer recurrence times. The lowered hydrogen composition lowers the CNO energy generation rate, requiring a higher pressure/temperature to get to the same level of burning as would be expected if $X = 0.70$. The lack of mass loss greatly affects the time the WD spends at high luminosities, since it must burn through most of the accreted envelope rather than removing most of it through winds. At high $\dot{M}$'s, the time spent on the high-luminosity branch is comparable to the time spent in quiescence, so ignoring mass loss will lead to appreciably longer recurence times. Additionally, the cores for Iben (1982) were typically much hotter than ours, exceeding the temperature of the quiescent helium layer from our models. We expect this would act to decrease the recurrence time since lower pressures (and thus accreted masses) are required at higher temperatures to trigger a TNR. Finally, Iben (1982) must certainly have used different opacities, which would affect the structure of the accreted envelope.

At first, data for a stripped AGB core with $T_c \approx 3 \times 10^8$ K is presented. For $\dot{M} = 2.5 \times 10^{-7}\, M_\odot\,{\rm yr}^{-1}$, he reports steady and stable burning, which we also observe. At $\dot{M} = 1.5 \times 10^{-7}\, M_\odot\,{\rm yr}^{-1}$, he observes recurrence times at around 72 years, though they are evidently still increasing in his Figure 6. In contrast, our corresponding model had a recurrence time of 42 years. His model has approximately 36 years of intense hydrogen burning, whereas ours burns for only 17, indicating that mass loss is responsible for the much of the discrepancy. He also displays data for the same hot WD as well as one whose core has gone into a "steady-state" temperature configuration ($T_c \approx 7 \times 10^7$ K) accreting at $\dot{M} = 1.5 \times 10^{-8}\, M_\odot\,{\rm yr}^{-1}$. These exhibit recurrence times of $\approx 550 - 650$ years, though it is apparent in his Figures 7 and 11 that the recurrence times have not grown to their asymptotic values yet. We observe longer recurrence times at ≈ 1400 years. In this case, the neglect of mass loss is likely unimportant since the accretion phase is much longer than the outburst phase, but the higher central temperatures of both WDs are pushing the recurrence times down relative to ours.

Livio et al. (1989) simulated a 1.0 $M_\odot$ WD with $T_c = 10^8$ K accreting at 10^{-8}, 10^{-7}, and 10^{-6} $M_\odot\,{\rm yr}^{-1}$. Again, this core temperature is even hotter than the stable burning temperature of the steady burners, so it will influence ignition masses. Thus, we would expect their results to exhibit shorter recurrence times and a lower stability boundary. Additionally, the accreted material in their simulations had $X = 0.7$ and $Z = 0.03$. Their M8 model, at $\dot{M} = 10^{-8}\, M_\odot\,{\rm yr}^{-1}$ exhibited repeated hydrogen flashes with $t_{\rm recur} = 1520$ years and an ignition mass (total mass present above the helium layer) of $\Delta M_{\rm ign} = 1.7 \times 10^{-5}\, M_\odot$. In our corresponding model which had the lower core temperature but the same $\dot{M}$, we find $t_{\rm recur} = 2220$ years and an ignition mass of $\Delta M_{\rm ign} = 2.6 \times 10^{-5}\, M_\odot$, which given the core temperature for such a relatively low $\dot{M}$, is a plausible difference.

For their M7 model, which accreted at 10^{-7} $M_\odot\,\mathrm{yr}^{-1}$, they found $t_{\rm recur} = 135$ years, whereas our corresponding model gives $t_{\rm recur} = 73$ years. Their M6 model, accreting at 10^{-6} $M_\odot\,\mathrm{yr}^{-1}$ expanded to red giant proportions, as did ours.

Cassisi et al. (1998) studied WDs with $M_{\rm WD} = 0.516\ M_\odot$ and $M_{\rm WD} = 0.80\ M_\odot$ accreting at rates comparable to the stable burning regime. Their accreting matter has $X = 0.7$ and $Z = 0.02$, and the core temperatures are well below their observed helium layer temperatures, so we expect their models to compare more favorably to ours. It appears that there was no mass loss prescription applied by Cassisi et al. (1998). We don't anticipate this causing any significant differences with our results since the stable burning lifetimes for the configurations in question are small compared to the accretion timescales. Additionally, the opacities used in Cassisi et al. (1998) are taken from older Los Alamos tables that they claim are very similar to the OPAL opacities. They simulated a $0.516\ M_\odot$ WD accreting at rates of 2×10^{-8}, 4×10^{-8}, 6×10^{-8}, 10^{-7}, and 10^{-6} $M_\odot\,\mathrm{yr}^{-1}$. They observe that the model with $\dot{M} = 2\times10^{-8}\ M_\odot\,\mathrm{yr}^{-1}$ exhibits hydrogen flashes with $t_{\rm recur} = 5400$ years, whereas our $0.51\ M_\odot$ model at the same $\dot{M}$ has $t_{\rm recur} = 5040$ years. For $\dot{M} = 4\times10^{-8}$, 6×10^{-8}, and 1×10^{-7} $M_\odot\,\mathrm{yr}^{-1}$, they observe steady burning, which is mostly consistent with our results, though we found that for our $0.51\ M_\odot$ WD, an $\dot{M}$ of 10^{-7} $M_\odot\,\mathrm{yr}^{-1}$ resulted in a red giant configuration. Their WD is slightly more massive, and given that we find that $\dot{M} = 9\times10^{-8}\ M_\odot\,\mathrm{yr}^{-1}$ gives stable burning on our $0.51\ M_\odot$ WD, the discrepancy seems plausible. Finally, both Cassisi et al. (1998) and we observe a red giant phase for $\dot{M} = 1\times10^{-6}\ M_\odot\,\mathrm{yr}^{-1}$.

For their $0.80\ M_\odot$ WD, Cassisi et al. (1998) ran simulations with $\dot{M} = 10^{-8}$, 4×10^{-8}, 10^{-7}, 1.6×10^{-7}, and 4×10^{-7} $M_\odot\,\mathrm{yr}^{-1}$. For the lowest three $\dot{M}$'s, they found $t_{\rm recur} = 3110$ years, 483 years, and 204 years, respectively. For the same mass and $\dot{M}$'s, we find $t_{\rm recur} = 3370$, 596, and 200 years, respectively. We both observe steady burning at $\dot{M} = 1.6\times10^{-7}\ M_\odot\,\mathrm{yr}^{-1}$, and we both observe a red giant configuration at $\dot{M} = 4\times10^{-7}\ M_\odot\,\mathrm{yr}^{-1}$.

Finally, we compare to Yaron et al. (2005), who simulated accreting WDs with masses of 0.65, 1.00, and 1.25 $M_\odot$ (among others that we do not compare to). For each of these masses, they accreted matter at rates of 10^{-8} and 10^{-7} $M_\odot\,\mathrm{yr}^{-1}$ (again with many more at lower $\dot{M}$'s that aren't applicable to our study). They also varied the core temperature between 1×10^7 K and 5×10^7 K. It shouldn't affect our results, but we will compare only with the $T_c = 3\times10^7$ K results. Finally, they employed an optically thick, supersonic wind as a mass loss prescription (Prialnik & Kovetz 1995) and allowed for convective overshoot, as evidenced by their metal-enriched ejecta.

At no point is stable burning reported in Yaron et al. (2005), though it seems that simulations with no mass loss correspond to our red giant or stable configurations (a period is still reported in their Table 3). For $M_{\rm WD} = 0.65\ M_\odot$, $t_{\rm recur} = 10200$ and 254 years are reported for $\dot{M} = 10^{-8}$ and 10^{-7} $M_\odot\,\mathrm{yr}^{-1}$, respectively. Using our own $0.65\ M_\odot$ WD, we find a recurrence time of 7800 years for $\dot{M} = 10^{-8}\ M_\odot\,\mathrm{yr}^{-1}$ and stable burning for $\dot{M} = 10^{-7}\ M_\odot\,\mathrm{yr}^{-1}$. For the $1.00\ M_\odot$ case, the two reported $t_{\rm recur}$'s are 2030 and 87.4 years, whereas ours are $t_{\rm recur} = 2216$ and 72.6 years. Finally, their $1.25\ M_\odot$ WDs give $t_{\rm recur} = 384$ and 19.6 years. Our $1.25\ M_\odot$ WD models indicate $t_{\rm recur} = 258$ and 14.4 years at these $\dot{M}$'s. For the higher $\dot{M}$'s, there is little to no metal enrichmeent in the ejecta and only minor helium enrichment, so we expect the reasonable agreement in most of the calculations. The exception is the $M = 1.25\,M_\odot$, $\dot{M} = 10^{-8}\,M_\odot\,\mathrm{yr}^{-1}$ calculation, where the ejecta in Yaron et al. (2005) is significantly metal-enriched, indicating dredge-up from the core. It's not immediately obvious why our calculation with no enrichment has a shorter recurrence time, since CNO burning should start more easily with an enriched base layer.

6. POST-OUTBURST NOVAE

In addition to the models computed for stability analysis, we also ran models with $M_{\rm WD} = 0.6\,M_\odot$, $1.0\,M_\odot$, $1.1\,M_\odot$, $1.2\,M_\odot$, $1.3\,M_\odot$, and $1.34\,M_\odot$ at a lower accretion rate of $\dot{M} = 10^{-9}\,M_\odot\,\mathrm{yr}^{-1}$ to study the stable burning phase after a classical nova (CN). For mass loss, we used both the super Eddington wind prescription described earlier as well as Roche lobe overflow (RLOF) by putting the WDs in a binary systems with Roche lobe radii between $R_{\rm RL} = 0.4\,R_\odot$ and $1.0\ R_\odot$. Our choice for the accretion rate, masses, and orbital separation was motivated by the study of the classical novae population by Townsley & Bildsten (2005). They showed that the observed orbital period distribution of the CNe was consistent with expectations of the mass transfer rate history of cataclysmic variables. This implied that the most often observed CNe would be those in 4-7 hours orbital periods with a mass transfer rate driven by magnetic braking at $10^{-9}\,M_\odot\,\mathrm{yr}^{-1}$. These tight orbits then enable Roche lobe overflow when the WD undergoing the CN reaches a photospheric radius $R_{\rm WD} = R_{\rm RL}$, triggering the mass loss from the WD that creates a common envelope. Within `MESA` this mass loss is simulated by eliminating any mass beyond the Roche lobe radius, effectively demanding that the WD photosphere not exceed $R_{\rm RL}$. It is simply the hydrostatic expansion of the actively burning layer that pushes the outer layers beyond $R_{\rm RL}$. Once the hydrogen layer mass has reduced to a value where $R_{\rm WD} \lesssim R_{\rm RL}$, the mass loss ends and the period of prolonged stable burning ensues. Since the ignition masses are smaller on more massive WDs, the expectation is that, even though rarer, more massive WDs will be more prevalent in the observed population.

Kato & Hachisu (1994) have accounted for mass loss in novae through optically thick winds driven by an opacity bump at $\log T(\mathrm{K}) \approx 5.2$ from the OPAL tables. This bump in opacity should cause a decrease in the Eddington luminosities, making our super Eddington wind prescription a plausible mass loss mechanism. We present results using both mass loss mechanisms independently, but it's likely that some combination of winds and Roche lobe overflow are present in actual novae. Finally, we again neglect convective dredge-up and the accompanying metal enrichment of the burning layer.

The evolutionary tracks of our $0.6\,M_\odot$, $1.0\,M_\odot$, $1.2\,M_\odot$, and $1.3\,M_\odot$ models just after the end of mass loss are shown on the HR diagram with respect to the

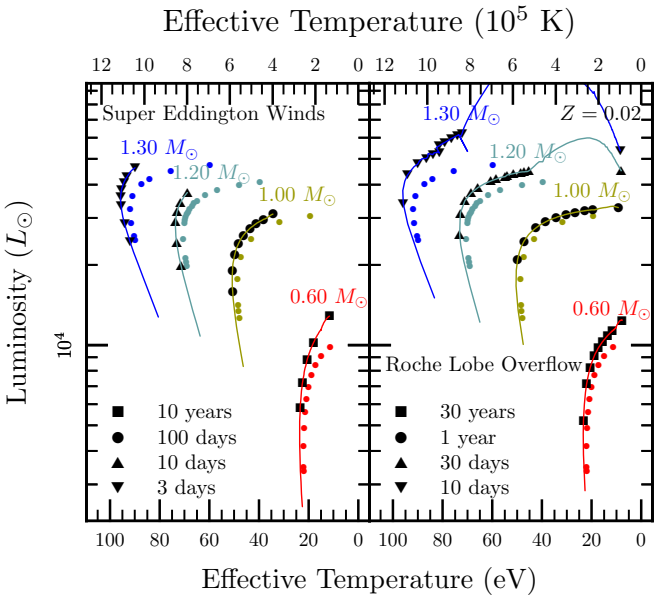

Figure 10. The paths of the CNe through the HR diagram after outburst (lines) with the static positions of the steadily-burning models presented earlier (circles). Models using super Eddington winds are on the left, and those using RLOF are on the right. For both mass loss mechanisms, we divide the tracks into equal time portions with markers whose time lengths are indicated in the legend.

stable burners of §3 for both mass loss prescriptions in Figure 10. There we show the CNe as lines with markers on them denoting equal time steps after mass loss has ended. For instance, the RLOF 0.60 $M_\odot$ model burns steadily for approximately 250 years, whereas our RLOF 1.20 $M_\odot$ model only does so for approximately a year. The duration of the supersoft source (SSS) phase is clearly dependent on both the WD mass and the amount of mass ejected. The super Eddington wind models tend to start "later" in the steady-state locus since the super Eddington winds remove more mass than RLOF. As a result, those turn-off times are always shorter than the those of the corresponding RLOF models. We found there is some cutoff mass that depends on orbital parameters below which novae fill their Roche lobe before the luminosity goes super Eddington. For the models shown, the 0.6 $M_\odot$ and 1.0 $M_\odot$ fill their Roche lobes before going super Eddington, so the RLOF prescription is likely more accurate. For the higher masses, the Roche lobe is bigger, allowing for greater expansion, leading to lower envelope temperatures, greater opacities, and thus a lower Eddington limit. The super Eddington models for these higher masses never expanded to the Roche lobe radius set for the RLOF models. Additionally, we can see that during the contracting phase, the RLOF 1.2 $M_\odot$ and 1.3 $M_\odot$ WDs are super Eddington (the upwards excursion), so the mass loss in those cases is certainly a lower limit.

After mass loss (on the far red end of each evolutionary track), each CN passes near or directly through the locus of stably burning phases corresponding to its mass. However, at an accretion rate of $\dot{M} = 1.0 \times 10^{-9}\, M_\odot\, \mathrm{yr}^{-1}$, the stable burning consumes hydrogen faster than it is accreted. Thus, a CN passes through phases with a progressively smaller hydrogen layer, tracing a path to and around the knee until the layer becomes thinner than that of the critically stable WD configuration. Sala & Hernanz (2005) modeled CNe in the post-outburst phase as a series of stably-burning WDs and tracked their evolution for four envelope compositions. Their Figure 1 gives HR diagram paths as well as the evolution of the hydrogen-rich layer in each of their modeled CNe. Their asymptotic luminosities and effective temperatures for the most metal-poor configuration (ONe25, at $Z_{\rm env} = 0.25$) agree well with our stable burners, though we find that the CNe themselves follow tracks that are marginally brighter and hotter than the corresponding stable burners. The depleting hydrogen layer is very apparent in Figure 11, where we see that the WDs using RLOF realize states with hydrogen masses and $T_{\rm eff}$'s very close to the corresponding steadily burning WDs. However, the WDs using super Eddington winds typically removed more mass than the RLOF models, so they "skip" some or most of the steady-state configurations and instead start with a much lower envelope mass. This disparity in the amount of fuel between the two configurations at the same mass explains why the turn-off times are much shorter for super Eddington winds than RLOF. In either cases, hydrogen burning becomes an insignificant source of luminosity past the lowest M stable burner state, and the WD then proceeds down the WD cooling track at nearly constant radius and hydrogen mass. Comparing to the ONe25 model in Sala & Hernanz (2005), we observe turn-off times that are always longer in the RLOF and low-mass super Eddington cases. For the higher mass super Eddington models, we observe marginally shorter turn-off times, likely driven by the skipped steady-state modes. The overall trend is that nearly all turn-off times in Sala & Hernanz (2005) are shorter than ours due to the significant metal enrichment of their envelopes, which is an important difference we elaborate on later.

Figure 12 shows the temperature profile of the 1.0 $M_\odot$ CN at four distinct stages: the low luminosity accreting state, the peak of hydrogen burning during the TNR, the point of highest $T_{\rm eff}$, which is near the end of stable burning, and the cooling/accumulating phase just after stable burning has ceased. For each profile, the location of the base of the hydrogen-burning layer (here approximated as the location where $X = 0.1$) is marked. For comparison, the lowest-$\dot{M}$ 1.00 $M_\odot$ stable burner is also shown in the gray line. As the hydrogen accumulates in the low-luminosity state, the profile is somewhat similar to a cooling WD, albeit with some heat still left over in the helium layer as well as some energy generation due to the compressional losses from accretion (see Figures 26 and 27 in Paxton et al. (2013)). Once the pressure at the base of the hydrogen reaches a critical threshold, the thermonuclear runaway (TNR) ensues, raising the temperature at the base to almost 2×10^8 K, which in turn drives a convective zone in the hydrogen layer. The radius then expands, triggering Roche lobe overflow until the envelope's thermal structure is reorganized so that it can carry the luminosity from the hydrogen burning. It then enters the stable burning phase, during which we see a temperature profile in the hydrogen-rich layer that is very similar to a steadily burning WD. Note that between the TNR and the SSS phase, approximately 90 percent of the hydrogen layer has been lost. A small

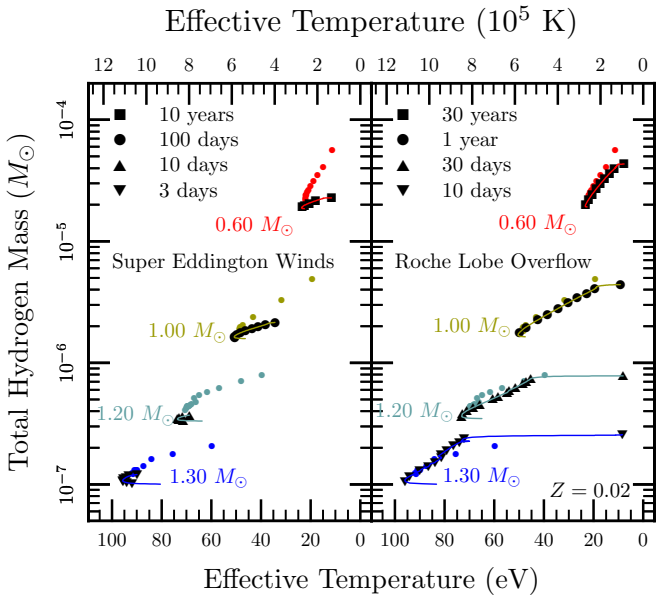

Figure 11. The hydrogen mass against the effective temperature of post-outburst CNe (lines) compared to steady burners of the same mass (circles). Models using super Eddington winds are on the left and those using RLOF are on the right. The RLOF novae pass through phases closely resembling their steadily-burning counterparts at the same effective temperatures, but the stronger mass loss from super Eddington winds cause novae to start stable burning at a much lower envelope mass than the corresponding RLOF models. Equal time markers are the same as mentioned in Figure 10.

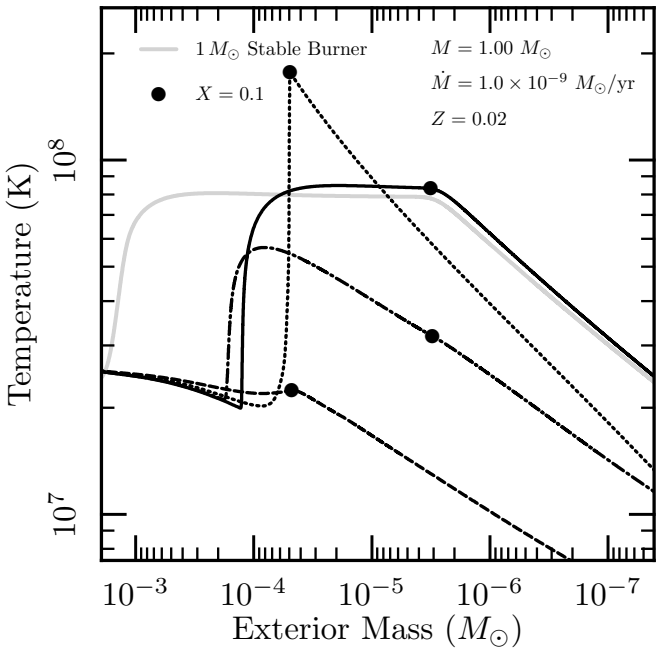

Figure 12. Time series of temperature profiles in a 1.00 $M_\odot$ WD accreting solar material at $\dot{M} = 1.0 \times 10^{-9}\ M_\odot\ \mathrm{yr}^{-1}$ with RLOF for mass loss. The point shows the base of the H layer. The long-dashed line is just prior to the outburst, when the luminosity is low and due primarily to compressional heating. The dotted line is the profile at the time of peak hydrogen burning, with a vigorously convective layer extending from the point of peak burning. The solid line is taken from the time at which $T_{\rm eff}$ is at a maximum, marking the end of the stable burning phase. The dash-dotted line is from shortly after the stable burning ceases, as the envelope is cooling off and accumulating hydrogen. The gray line is the profile of a 1.00 $M_\odot$ WD accreting at the lower stable limit.

portion of this is due to the stable burning, but the majority is due to RLOF. After stable burning ceases, the envelope cools and accretes hydrogen until the next TNR repeats the process.

Combined measurements of $T_{\rm eff}$ and the turn-off time of a CN (Henze et al. 2011) can be used to infer the WD mass. Figure 13 shows observed turn-off times and $T_{\rm eff}$'s in post-ouburst novae. Included in Figure 13 are data from M31 (Henze et al. 2011, 2013) and galactic sources (Rauch et al. 2010; Osborne et al. 2011; Beardmore et al. 2012). For the Henze et al. (2011) dataset, we've only included data that had reported uncertainties rather than limit points, which discriminates against longer-lived SSS phases since they are less likely to be observed from beginning to end. We also plot our calculations, where we define the turn-off time as the time between the beginning of mass loss and when the luminosity falls below one quarter of the peak luminosity of the stable burners of the same mass. This ending criteria isn't very crucial since the luminosity evolution after the stable burning phase is very rapid compared to time spent doing stable burning. For the computational models, we cannot report a single $T_{\rm eff}$ since it increases through most of the SSS phase. The turn-off time is well defined, so we report our results as a horizontal line in Figure 13 with the effective temperatures being those during the latter 70% of stable burning (the SSS is likely obscured at earlier times by the expanding ejecta shell).

The temperatures reported for the observed CNe are obtained either by approximating an X-ray spectrum as a blackbody (Henze et al. 2011, 2013) or through more sophisticated NLTE simulations (Rauch et al. 2010; Osborne et al. 2011; Beardmore et al. 2012). These two methods can yield different temperatures by $\approx 10\%$ (see Figure 4 from Henze et al. 2011), so there will necessarily be disagreement between CNe analyzed by the two different methods. Our models do not account for dredge-up and the subsequent metal enrichment of the ejecta and stably-burning envelope. This could cause two effects. First, the enriched TNR could burn more vigorously, driving stronger mass loss and thus shortening the turn-off time. Secondly, the remnant envelope after mass loss will be metal-enriched and will thus burn through the remaining hydrogen more quickly than if the same mass were at solar abundance, as shown in Sala & Hernanz (2005). Both of these factors indicate that our turn-off times are longest limits for the given mass loss prescriptions. We do not, however, expect metal enrichment to alter the effective temperature of the outburst, so these can still be used to constrain WD masses. Finally, the observed data shown in Figure 13 are deficient in low-temperature ($kT_{\rm BB} < 30\,$eV) events.

Such events do exist, but the available measured turn-off times for them are lower limits since they have not been observed for a long enough time to detect both turn-on and turn-off. Additionally, observing such events is difficult due to absorption by interstellar neutral hydrogen and the overall weaker X-Ray flux. Finally, such low-mass systems may be more numerous, but since their recurrence times are significantly longer than their higher-mass counterparts, they are observed less often. In Figure 13 we only plot those events from Henze et al. (2011) that have established uncertainties in both the blackbody temperature and the turn-off time. The agreement be-

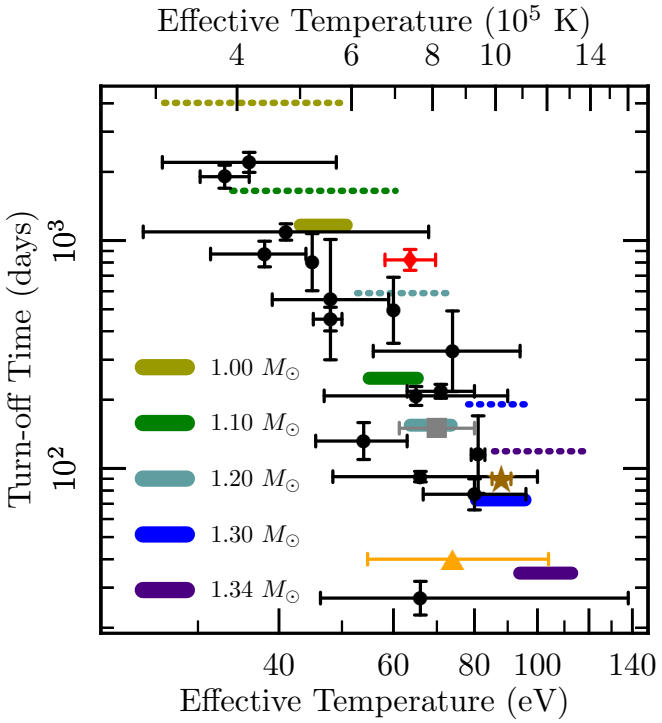

Figure 13. Turn-off time against $kT_{\rm eff}$ for observed CNe from the catalogue of M31 CNe in Henze et al. (2011) (black dots), the CN in globular cluster Bol 126 in M31 (Henze et al. 2013) (orange triangle), V4743 Sgr (Rauch et al. 2010) (red diamond), the recurrent nova RS Oph (Osborne et al. 2011) (brown star), HV Ceti (Beardmore et al. 2012) (gray square), as well as the results of our work. Solid lines represent the super Eddington wind models and the dotted lines represent RLOF models. The range of effective temperatures shown for the computational models are the temperatures during the latter 70% of the stable burning period. Note that the $T_{\rm eff}$ for the `MESA` simulations are from the Stefan-Boltzmann law given a luminosity and a photospheric radius. $T_{\rm eff}$'s from Henze et al. (2011, 2013) are blackbody approximations taken from X-Ray spectra, and $T_{\rm eff}$'s from the galactic novae are from NLTE models of hot WD atmospheres. These temperatures can differ by $\approx 10\%$ due to radiative transfer effects.

tween theory and observation in this region of parameter space is strong, implying that most of the novae with SSS phases that have established turn-off times and blackbody temperatures have $M \geq M_\odot$. As X-ray monitoring of M31 continues, more SSS's will turn off and stacked pointings allow for detection of fainter SSS's. Thus we will soon be able to probe more reliably into the lower-mass regime (Henze 2013, private communication).

Due to the variability of $T_{\rm eff}$ during the SSS phase, it is not an ideal tracer of WD mass on its own. The turn-off time, however, is a function of the luminosity and hydrogen mass layer size, assuming the mass loss history is known. Since we've seen that $\Delta M_{\rm H}$ decreases with increasing $M_{\rm WD}$ while L increases with increasing $M_{\rm WD}$, the turn-off time should be a consistent tracer of WD mass while also being relatively easy to measure. Using our high-mass CNe models, including an additional $1.34\,M_\odot$ CN, we find power laws relating turn-off time to WD mass given by $M_{\rm WD} = 1.20\,M_\odot\,(513\text{ days}/t_{\rm off})^{0.081}$ (for RLOF) and $M_{\rm WD} = 1.20\,M_\odot\,(137\text{ days}/t_{\rm off})^{0.089}$ (for super Eddington winds). We then apply this relation to the catalogue of Henze et al. (2011) to get corresponding WD masses to compare to the reported ejection masses, which were inferred by Henze et al. (2011) from

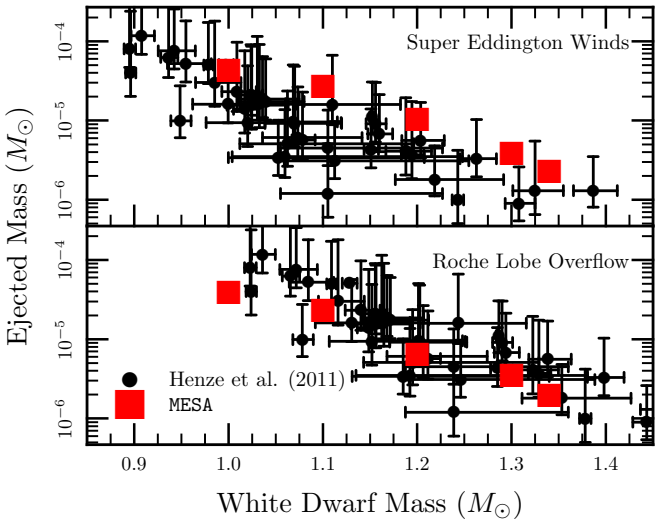

Figure 14. Ejected mass in a nova as a function of WD mass for both the `MESA` simulations as well as the same catalogue of observations used in Figure 13. The masses for the observed data were obtained by using a power law fit from the simulated data to convert turn-off times to masses.

the turn-on time and the ejecta velocity. The results of this analysis are shown in Figure 14. We see the mapping from turn-off time to $M_{\rm WD}$ gives a similar relation between WD mass and ejected mass as the simulations for either mass loss prescription. Note though that the RLOF law gives super-Chandrasekhar mass WDs for sufficiently low turn-off times, which is a result of the underprediction of mass loss in high-mass WDs in the RLOF assumption.

7. CONCLUDING REMARKS

We have presented stably burning WD models, found the lowest M's that permit such stable burning, and verified that they are consistent with other time-dependent studies as well as time-independent linear analysis studies of stability. We've shown that the hot helium ash left over from hydrogen burning dominates the thermal structure of both stably and unstably burning WDs at high M's. This helium layer is important because it sets the recurrence times for rapidly accreting recurrent novae where dredge up is unable to reach the WD core, but it is also important because it is likely to ignite unstably once it has grown large enough. The mass of helium in the WD, $\Delta M_{\rm He}$, is not a static property of a stably burning model. For the $1.00\,M_\odot$ example shown in Figure 4, $\Delta M_{\rm He} \approx 1.5 \times 10^{-3}\,M_\odot$, but it will continue to grow at the accretion rate, $\dot{M}$, until the pressure and the temperature at the base become high enough to initiate unstable helium burning. Sienkiewicz (1980), Iben & Tutukov (1989), and Cassisi et al. (1998) showed that the stable burning regimes for hydrogen and helium are mutually exclusive for the case of solar composition accretion. However, Yoon et al. (2004) offer a way to merge the two stability regimes if a large amount of differential rotation is allowed in the burning shells. Our calculations assume no rotation, and we observed unstable helium burning for WDs that were allowed to continuously accrete.

Finally, we showed how CNe pass through the stably burning phases after their outburst and subsequent mass loss. The duration of this SSS phase is highly sensitive to

the mass of the underlying WD, spanning for hundreds of years for $M_{\rm WD} \approx 0.60\ M_{\odot}$ to mere tens of days for $M_{\rm WD} \approx 1.30\ M_{\odot}$. This variety of durations indicates a mapping from observed turn-off times to WD mass, though a study of the effects of metal enhancement and a better understanding of mass loss is necessary to get a more precise relationship.

We thank Ken Nomoto for helpful discussions regarding the calculations in Nomoto et al. (2007). Additionally we thank Pablo Marchant for his useful binary Roche lobe overflow routines that were used in this work and Jeno Sokoloski for consultation regarding RNe observations. Finally, we thank Martin Henze and the referee for very helpful comments. Most of the simulations for this work were made possible by the Triton Resource. The Triton Resource is a high performance research computing system operated by the San Diego Supercomputer Center at UC San Diego. This work was supported by the National Science Foundation under grants PHY 11-25915, AST 11-09174 and AST 12-05574.

REFERENCES

Beardmore, A. P., Osborne, J. P., Page, K. L., et al. 2012, A&A, 545, 116
Cassisi, S., Iben, I. J., & Tornambe, A. 1998, ApJ, 496, 376
Denissenkov, P. A., Herwig, F., Bildsten, L., & Paxton, B. 2013, ApJ, 762, 8
Fujimoto, M. Y. 1982, ApJ, 257, 767
Gallagher, J. S., & Starrfield, S. 1978, ARA&A, 16, 171
Hachisu, I., & Kato, M. 2010, ApJ, 709, 680
Hachisu, I., Kato, M., & Nomoto, K. 1996, ApJL, 470, L97
Hansen, C. J., Kawaler, S. D., & Trimble, V. 2004
Henze, M., Pietsch, W., Haberl, F., et al. 2011, ApJ, 533, A52
—. 2013, A&A, 549, 120
Iben, I. J. 1982, ApJ, 259, 244
Iben, I. J., & Tutukov, A. V. 1989, ApJ, 342, 430
Iglesias, C. A., & Rogers, F. J. 1993, ApJ, 412, 752
—. 1996, Astrophysical Journal v.464, 464, 943
Kato, M., & Hachisu, I. 1994, ApJ, 437, 802
Kovetz, A., & Prialnik, D. 1994, ApJ, 424, 319
Livio, M., Prialnik, D., & Regev, O. 1989, ApJ, 341, 299
Lodders, K. 2003, ApJ, 591, 1220
Nomoto, K. 1982, ApJ, 253, 798
Nomoto, K., Nariai, K., & Sugimoto, D. 1979, PASJ, 31, 287
Nomoto, K., Saio, H., Kato, M., & Hachisu, I. 2007, ApJ, 663, 1269
Nomoto, K., Thielemann, F. K., & Yokoi, K. 1984, ApJ, 286, 644
Osborne, J. P., Page, K. L., Beardmore, A. P., et al. 2011, ApJ, 727, 124
Paczynski, B. 1970, Acta Astronomica, 20, 47
—. 1983, ApJ, 264, 282
Paczynski, B., & Zytkow, A. N. 1978, ApJ, 222, 604
Paxton, B., Bildsten, L., Dotter, A., et al. 2011, ApJS, 192, 3
Paxton, B., Cantiello, M., Arras, P., et al. 2013, ApJS, 208, 4
Piersanti, L., Cassisi, S., Iben, I. J., & Tornambe, A. 1999, ApJ, 521, L59
Prialnik, D., & Kovetz, A. 1995, ApJ, 445, 789
Rauch, T., Orio, M., Gonzales-Riestra, R., et al. 2010, ApJ, 717, 363
Sala, G., & Hernanz, M. 2005, A&A, 439, 1061
Schaefer, B. E. 2010, ApJS, 187, 275
Schwarz, G. J., Ness, J.-U., Osborne, J. P., et al. 2011, ApJS, 197, 31
Shara, M. M., Prialnik, D., & Kovetz, A. 1993, ApJ, 406, 220
Shen, K. J., & Bildsten, L. 2007, ApJ, 660, 1444
Sienkiewicz, R. 1980, A&A, 85, 295
Sion, E. M., Acierno, M. J., & Tomczyk, S. 1979, ApJ, 230, 832
Starrfield, S., Sparks, W. M., & Truran, J. W. 1974, ApJS, 28, 247
Townsley, D. M., & Bildsten, L. 2004, ApJ, 600, 390
—. 2005, ApJ, 628, 395
Tuchman, Y., & Truran, J. W. 1998, ApJ, 503, 381
van den Heuvel, E. P. J., Bhattacharya, D., Nomoto, K., & Rappaport, S. A. 1992, A&A, 262, 97
Yaron, O., Prialnik, D., Shara, M. M., & Kovetz, A. 2005, ApJ, 623, 398
Yoon, S. C., Langer, N., & van der Sluys, M. 2004, A&A, 425, 207